ChemComm

Accepted Manuscript

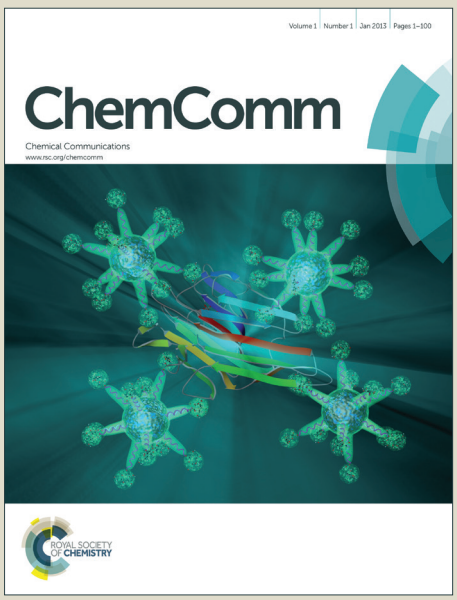

ROYAL SOCIETY OF CHEMISTRY

www.rsc.org/chemcomm

Cite this: DOI: 10.1039/c0xx00000x

www.rsc.org/xxxxxx

COMMUNICATION

Novel Bimetallic Core–Shell Nanocrystal/Clay Composites with Superior Catalytic Activities

Dharmesh Varade, and Kazutoshi Haraguchi*

Received (in XXX, XXX) Xth XXXXXXXXX 20XX, Accepted Xth XXXXXXXXX 20XX
DOI: 10.1039/b000000x

Clay (synthetic hectorite; Laponite XLG) plays a very crucial role in the formation and stabilization of core–shell nanocrystals and affords high stability, large BET surface area and stimulates the exceptional catalytic activity of the core–shell NCs.

Bimetallic core–shell nanocrystals (NCs) are emerging as highly important materials with attractive possibilities for the effective tuning of their properties, which are different from those of monometallic NCs.[1] In particular, Pt-, Pd-, and Au-based core–shell NCs with controlled sizes and shapes have promising optical and catalytic activities.[2-4] A large variety of core–shell NCs with a wide range of applications are available.[1a] However, despite the impressive advances in the design and preparation of these core–shell NCs, there is a serious paucity of less intricate, more explicit, and universal methodologies for their fabrication. Consequently, a simple and direct method for the production of new core–shell-structured catalyst systems with designed compositions and improved properties is highly desirable for the development of innovative multifunctional smart materials, but this remains a significant challenge.

Clay minerals have been used to prepare various types of functional nanomaterials. The well-established use of clay to interact with drugs and other biological molecules for controlled delivery[5a,5b] and the ability of clays to interact with polymers to enhance their mechanical properties, as seen in the development of polymer–clay nanocomposites and nanocomposite gels, are important applications.[5c-5e] Moreover, we recently showed that the inclusion of clay might play a crucial role in imparting high stability, large Brunauer–Emmett–Teller (BET) surface areas, and promising multifunctionalities to the resulting Pt/clay composite materials.[6] In addition, there have been several reports of monometallic NCs using clays such as montmorillonite, laponite, or aminoclays.[7] However, no bimetallic NCs with clay have been produced to date because of the complexity of their preparation.

In the present communication, we report a new clay-mediated one-pot preparation of various bimetallic core–shell NCs with well-defined shapes and unique catalytic features. This leads to the formation of core–shell NC/clay composite materials that are expected to incorporate several different functionalities in one structure; this is difficult to achieve in single-component materials. Moreover, this synthesis affords a convenient and environmentally benign route to large-scale production (display same characteristics even when production is scaled up) because it does not require high temperatures, organic additives, or electrochemical deposition. These features undoubtedly make these core–shell NC/clay composite materials promising for various practical and industrial applications.

The core–shell NC/clay composites were prepared using a facile wet-chemical reduction method (see the Supporting Information for details). First, a stable aqueous dispersion of exfoliated clay platelets (2 wt%) was prepared; the dispersion was homogeneous, nearly transparent, and had a fairly high pH (10.2) and zeta potential (−37.1 mV) as a result of the negatively charged two-dimensional silicate nanosheets.[6a] In a typical synthesis of Pd–Pt core–shell NCs (Pt/Pd molar ratio = 1.0), K_2PtCl_4 solution (1 mL; 20 mM) and K_2PdCl_4 solution (1 mL; 20 mM) were mixed with a clay dispersion (1 mL; 2 wt%) in a vial to give a homogenous mixture (**Figure S1a** in the Supporting Information). The precursor ions interacted with the clay platelets on mixing, and then addition of a freshly prepared aqueous solution of ascorbic acid (0.5 m; 0.4 M) induced coreduction of the metal ions in the presence of clay. A similar method was used to prepare Au–Pt and Au–Pd core–shell NCs. In contrast, when the reaction was performed in the absence of clay under otherwise identical synthetic conditions, severe particle aggregation was observed in all the systems, as shown in **Figure S1b** for Pd–Pt, unambiguously showing that the clay played a pivotal role as an efficient stabilizer in the production of bimetallic core–shell NCs.

A representative low-magnification transmission electron microscopy (TEM) image of the as-prepared Pd–Pt NCs (Pd/Pt molar ratio = 1.0), presented in **Figure 1a**, shows the successful formation of uniform and spherical bimetallic Pd–Pt NCs of size *ca*. 60–70 nm with a well-defined morphology. The high-resolution TEM (HRTEM) image shows that these NCs have good crystallinity with well-defined fringes (**Figure 1b**: shell region). The periodicity of the lattice is approximately 0.21 nm, which coincides with the (111) *d*-spacing of Pt face-centered cubic (*fcc*) crystals.[2b] The corresponding selected-area electron diffraction patterns (inset; **Figure 1b**) showed ring arrays with intense spots assigned to the (111), (200), (220), and (311) planes of Pt *fcc* crystals showing the polycrystalline nature of Pt. The high-angle annular dark-field scanning TEM (HAADF-STEM)

image in **Figure 1c** shows a clear contrast between the core and the shell in the Pd–Pt structural morphology; the brighter core coated by a darker shell in each particle is perfect in the HAADF-STEM image, validating this method as a direct and feasible way of creating core–shell hybrid nanostructures with a high content and good dispersion of metals. An energy dispersive X-ray spectroscopy (EDX) along a single Pd-Pt NC, indicated by the square in Figure 1c, is depicted in Figure 1d (elemental distributions); this compositional profile is consistent with a core–shell NC morphology in which the Pt count (orange line) decreases from the center of the particle with respect to Pd (blue line).

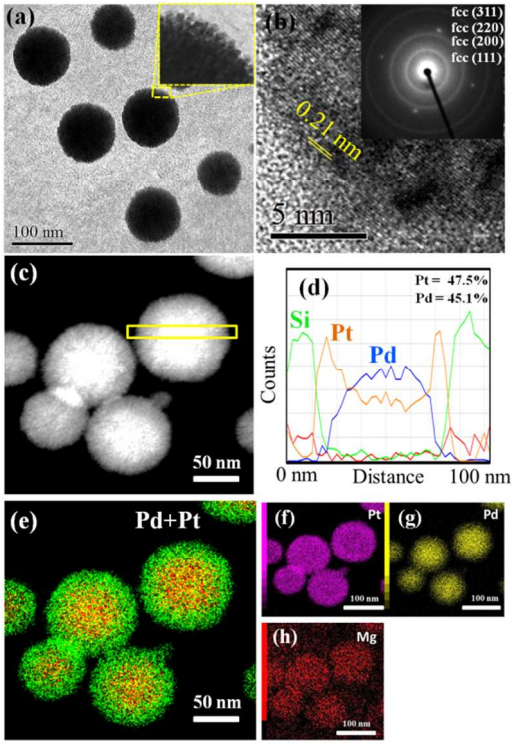

Fig. 1 (a) Low-magnification transmission electron microscopy (TEM) image and magnified image (inset) of nanoporous Pt shell. (b) High-resolution TEM image of bimetallic Pd–Pt core–shell NCs. The periodicity of the lattice is approximately 0.21 nm; inset shows selected-area electron diffraction pattern assigned to the (111), (200), (220), and (311) planes of Pt *fcc* crystals. (c) High-angle annular dark-field scanning TEM image of bimetallic Pd–Pt core–shell NCs. (d) Elemental distribution along a single NC, indicated by the square in part (c). Energy-dispersive X-ray mapping indicates (e) overlay of Pt and Pd and the presence of (f) Pt, (g) Pd, and (h) Mg.

EDX analysis of the NCs (**Figures 1d** and **1h**) confirms the presence of clay platelets (the signals for Si and Mg respectively) concentrated on the surface of the bimetallic NCs, imparting high stability by inhibiting coarsening of the NCs. The presence of Pt and Pd **(Figures 1f** and **1g)** and the overlay EDX mapping of Pt and Pd displayed in **Figure 1e** also indicate a clear separation of the two elements, with a Pd-rich core and a Pt-rich shell, thus confirming the formation of clay and bimetallic Pd–Pt core–shell NC composite materials. Importantly, it was noted that the Pt outer shell was in an interconnected tendril form, which provided nanoporosity in the outer-shell regions (inset; **Figure 1a**). Because Pd and Pt ions have very different reduction potentials vs. SHE (Pd = +0.987 eV and Pt = +0.76 eV) the reduction of Pd ions preferentially occurs in a short time to produce Pd cores. This is followed by overgrowth of Pt dendrites on Pd seeds in the presence of clay. The interaction between the clay surface and the Pt[6a] could form cavities and then facilitate the formation of nanoporous Pt shells on Pd cores. In addition, the wide-angle X-ray diffraction (XRD) patterns of the Pd–Pt core–shell NCs show multiple diffraction peaks, which can be indexed to the *fcc* lattices of Pt and Pd crystals (**Figure S2a**).[8]

These results imply that the formation of bimetallic core–shell NCs is the result of control of nucleation and prevention of metal cluster–cluster mutual contact by clay platelets.[7c] The exfoliated clay platelets, which have high aspect ratios and highly charged surfaces, generate a stable pseudo-cross-linked network in the presence of metal ions, as revealed by the increase in the viscosity (**Figure S3**). Addition of ascorbic acid induces the controlled reduction of metal ions near the clay surface, in which the clay plays an important role in the spontaneous separation of the deposited Pd and Pt, resulting in the one-pot formation of Pd–Pt core–shell NCs with an inner Pd core and an outer nanoporous Pt shell. Furthermore, the clay interacts with NCs and counteracts the inherent van der Waals attractions among the spherical core–shell NCs, preventing their random growth. In the absence of clay, the reduced Pt and Pd metals formed large inhomogeneous aggregates without defined structures (**Figure S1b(ii)**, inset). Also, by using clay, the use of organic components can be circumvented. It is therefore inferred that clay plays a pivotal role in the fabrication of bimetallic core–shell NCs with nanoporous outer shells; this is otherwise very challenging to achieve. Moreover, such core–shell NCs with nanoporous outer shells make it easy for guest species to access the inner cores, increasing the benefits of these core–shell structures in various applications.

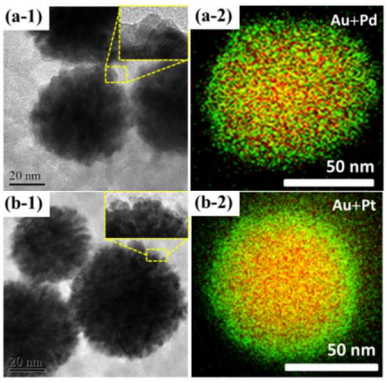

Fig. 2 (a-1) Low-magnification transmission electron microscopy (TEM) image of Au–Pd core–shell bimetallic NCs. Inset shows highly magnified image of shell region. (a-2) Energy-dispersive X-ray spectroscopy (EDX) elemental mappings of Au, Pd, and overlay of Au and Pd. (b-1) Low-magnification TEM image. Inset shows highly magnified image of shell region. (b-2) EDX elemental mappings of Au, Pt, and overlay of Au and Pt, indicating formation of Au–Pt core–shell NCs.

To further explore the full potential of this new approach, we also prepared other bimetallic NCs such as Au–Pd (**Figure 2a**) and Au–Pt (**Figure 2b**) in a similar fashion. These NCs are technically difficult to prepare using conventional methods, which use surfactants, because it is difficult to control the morphology. The representative TEM images in **Figures 2(a-1)**

and **2(b-1)** demonstrate the successful formation of well-defined Au–Pd and Au–Pt core–shell NCs using the proposed procedure. The corresponding EDX measurements, shown in **Figures 2(a-2)** and **2(b-2)**, show the composition and separation of the two elements, with an Au-rich core and a Pd- or Pt-rich shell in Au–Pd and Au–Pt core–shell NCs, respectively. As the inset of **Figure 2(a-1)** shows, reduction of the Au–Pd binary precursors led to the formation of smooth but curved Pd shells as a result of the small difference between the reduction potentials of the metal ions (0.013 eV), whereas Au–Pt forms a nanoporous Pt shell [inset; **Figure 2(b-1)**] similar to that discussed before because of the large difference between the reduction potentials of Au and Pt ions (Au = +1.00 eV, Pt = +0.76 eV). In the Au–Pd and Au–Pt core–shell NCs, the XRD patterns for individual metals could be readily distinguished, indicating a non-alloy structure, for instance, displaying both Au *fcc* and Pd *fcc* peaks for Au–Pd NCs (**Figure S2b**).[8] X-ray photoelectron spectroscopy (XPS) measurements for various bimetallic Pd–Pt, Au–Pt, and Au–Pd core–shell NCs also confirmed the presence of individual metallic Pt, Pd, and Au (**Figure S4**). Moreover, the inclusion of clay is a promising strategy for improving the specific surface areas of the resulting composite nanomaterials.[6a] N_2 adsorption–desorption measurements and analysis data show that core–shell NC/clay composites derived from the incorporation of nanoclay platelets have high BET surface areas (**Figure S5**).

To evaluate their activities, the novel composites were tested for the reduction of 4-nitrophenol with $NaBH_4$ in aqueous solution as a model system (**Figure 3a**).[4b] On addition of $NaBH_4$ to a 4-nitrophenol solution, the color changed from light yellow to an intense yellow, as a result of the formation of 4-nitrophenolate ions; accordingly, the absorption peak shifted from 317 to 400 nm (**Figure S6a**). The reduction of 4-nitrophenol with $NaBH_4$ did not proceed in the absence of a catalyst; the absorption intensity remained unaltered even after 90 min (**Figure S6b**). **Figures 3b–d** illustrate the reduction reaction of 4-nitrophenol, observed at different time intervals, using the core–shell NC/clay composites as catalysts. In the presence of a catalyst and $NaBH_4$, the 4-nitophenol was reduced, and the strong ultraviolet (UV) absorption peak at 400 nm rapidly diminished, depending upon the amount of catalyst used, demonstrating improved catalytic activity. In the reduction process, the overall concentration of $NaBH_4$ was much higher than that of 4-nitrophenol, so pseudo-first-order kinetics could be applied with respect to 4-nitrophenol in order to determine the catalytic activity. As expected, a linear correlation was obtained between $\ln(A_t/A_0)$ and reduction time (A_t and A_0 represent the absorbances at time t and of the initial 4-nitrophenolate ions, respectively; **Figure S7**); the slope provides the rate constant (k). In order to estimate the catalytic performances of the catalysts, the activity parameter $\kappa = k/m$ (the ratio of the rate constant to the total mass of catalyst added) was used. All these parameters are summarized in **Table 1**. It is inferred that a specific combination of different bimetals can significantly enhance the performance and activity of the catalyst. For instance, as shown by the data in **Table 1**, the Pd–Pt core–shell NC/clay composite (**Figure 3b**) was more active (κ = 1.70) than the Au–Pt core–shell NC/clay composite (κ = 0.53), as shown in **Figure 3c**. Furthermore, as can be seen from **Figure 3d**, the catalytic activity was significantly improved by using only 0.3 mg of Au–Pd core–shell NC/clay catalyst under similar conditions, with much higher activity (κ = 13.66). In comparison with Pt black (Table 1), the present core–shell NC/clay composites are highly beneficial for use as nanocatalysts, primarily because of their superior tolerance to undesirable agglomeration of active sites, as a result of the presence of clay.

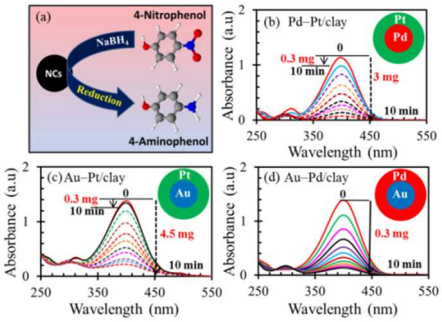

Fig. 3 (a) Model reaction showing reduction of 4-nitophenol to 4-aminophenol in presence of catalyst. Temporal evolution of ultraviolet-visible spectra for reduction of 4-nitrophenol by $NaBH_4$ in presence of (b) Pd–Pt/clay, (c) Au–Pt/clay, and (c) Au–Pd/clay composites. Insets show core–shell morphologies of composites.

Table 1: Summary of Activity Parameters, κ, Dependent on Rate Constants of Reactions (k) and Amounts of Catalysts Used

Catalyst	Weight m (mg)	Rate Constant k (s^{-1})	Activity Parameter κ ($s^{-1}g^{-1}$)
Pd–Pt/clay	3.0	5.1×10^{-3}	1.70
Au–Pt/clay	4.5	2.4×10^{-3}	0.53
Au–Pd/clay	0.3	4.1×10^{-3}	13.66
Pt Black	6.0	0.5×10^{-3}	0.08

In conclusion, this newly developed one-step synthesis rationally uses the spontaneous separation of deposited bimetals, resulting in the formation of several distinct bimetallic (Pd–Pt, Au–Pt, and Au–Pd) core–shell NC/clay composites. The clay plays a crucial role in the formation and stabilization of core–shell assemblies. This highly valuable and simple new synthetic route shows the high potential of the use of exfoliated clay platelets, affording new opportunities for tailoring bimetallic NC morphologies with designed compositions and structures. Intriguingly, the presence of clay provides high stability and a large BET surface area, and further improves the catalytic activity of the core–shell NC/clay composites. The results of this study will help in crafting more rational approaches to developing superior multifunctional catalysts using clay minerals.

This work was supported by the Ministry of Education, Science, Sports and Culture of Japan (Grant-in-Aid 23350117). The authors thank DIC analysis center (DIC Corp.) for the TEM-EDX, and XRD measurements.

References

1. a) R. G. Chaudhuri, S. Paria, *Chem. Rev.* **2012**, *112*, 2373–2433. b) J. H. Sinfelt, Bimetallic Catalysts: Discoveries, Concepts and Applications; John Wiley and Sons: New York, **1983**. c) X. Liu, X. Liu, *Angew. Chem. Int. Ed.* **2012**, *51*, 3311–3313.
2. a) B. Lim, M. Jiang, P. H. C. Camargo, E. C. Cho, J. Tao, X. Lu, Y. Zhu, Y. Xia, *Science* **2009**, *324*, 1302–1305. b) Y. Yamauchi, A. Tonegawa, M. Komatsu, H. Wang, L. Wang, Y. Nemoto, N. Suzuki,

K. Kuroda, *J. Am. Chem. Soc.*, **2012**, *134*, 5100–5109. c) C. Mingshu, K. Dheeraj, Y. Cheol-Woo, D. W. Goodman, *Science* **2005**, *310*, 291–293. d) A. M. Henning, J. Watt, P. J. Miedziak, S. Cheong, M. Santonastaso, M. Song, Y. Takeda, A. I. Kirkland, S. H. Taylor, R. D. Tilley, *Angew. Chem. Int. Ed.* **2013**, *52*, 1477–1480.

3. a) H. Zhang, M. Jin, J. Wang, W. Li, P. H. C. Camargo, M. J. Kim, D. Yang, Z. Xie, Y. Xia, *J. Am. Chem. Soc*. **2011**, *133*, 6078–6089. b) H. Zhang, M. Jin, H. Liu, J. Wang, M. J. Kim, D. Yang, Z. Xie, J. Liu, Y. Xia. *ACS Nano* **2011**, *5*, 8212–8222. c) A. X. Yin, X. Q. Min, Y. W. Zhang, C. H. Yan, *J. Am. Chem. Soc*. **2011**, *133*, 3816–3819. d) R. Narayanan, *Molecules* **2010**, *15*, 2124–2138.
4. a) J. Xu, T. White, P. Li, C. H. He, J. G. Yu, W. K. Yuan, Y. F. Han, *J. Am. Chem. Soc.*, **2010**, *132*, 10398–10406. b) G. J. Hutchings, M. A Haruta, *Appl. Catal. A* **2005**, *291*, 2–5. c) D. I. Enache, J. K. Edwards, P. Landon, B. Solsona-Espriu, A. F. Carley, A. A. Herzing, M. Watanabe, C. J. Kiely, D. W. Knight, G. J. Hutchings, *Science* **2006**, *311*, 362–365.
5. a) B. K. G. Theng, in *Developments in Clay Science*, Vol. *4* (Ed: B. K. G. Theng), Elsevier, Amsterdam, Netherlands **2012**, 245. b) J. I. Dawson, R. O. C. Oreffo, *Adv. Mater*. **2013**, *25*, 4069–4086. c) K. Haraguchi, T. Takehisa, *Adv. Mater*. **2002**, *14*, 1120–1124. d) K. Haraguchi, H. J. Li, *Angew.Chem. Int. Ed.* **2005**, *44*, 6500–6504. e) Q. Wang, J. L. Mynar, M. Yoshida, E. Lee, M. Lee, K. Okuro, K. Kinbara, T. Aida, *Nature* **2010**, *463*, 339–343.
6. a) D. Varade, K. Haraguchi, *Langmuir* **2013**, *29*, 1977–1984. b) D. Varade, K. Haraguchi, *Phys. Chem. Chem. Phys.,* **2013**, *15*, 16477–16480. c) D. Varade, H. Abe, Y. Yamauchi, K. Haraguchi, *ACS Appl. Mater. Interfaces* **2013**, *5, 11613−11617*
7. a) G. B. V. Varadwaj, K. M. Parida, *RSC Advances* **2013**, *3*, 13583–13593. b) K. K. R. Datta, M. Eswaramoorthy, C. N. R. Rao, *J. Mater*. Chem. **2007**, *17*, 613–615. c) N. Aihara, K. Torigoe, K. Esumi, *Langmuir* **1998,** *14*, 4945–4949.
8. S. E. Habas, H. Lee, V. Radmilovic, G. A. Somorjai, P. Yang,. *Nat. Mater*. **2007**, *6*, 692–697.

Material Chemistry Laboratory, Kawamura Institute of Chemical Research, 631 Sakado, Sakura, Chiba 285-0078, Japan; E-mail:hara@kicr.or.jp

† Electronic Supplementary Information (ESI) available: [TEM, Optical images, XRD and XPS measurements]. See DOI: 10.1039/b000000x/

